Letter of Intent for an Experiment at the Spallation Neutron Source

Precise Measurement of the Neutron Beta Decay Parameters "*a*" and "*b*"

The *Nab* Experiment

R. Alarcon
Arizona State University

J.D. Bowman (Spokesman), S.I. Penttilä, and W.S. Wilburn
Los Alamos National Laboratory

J.R. Calarco and F.W. Hersman
University of New Hampshire

T.V. Cianciolo, K.P. Rykaczewski, and G.R. Young
Oak Ridge National Laboratory

V. Gudkov
University of South Carolina

G.L. Greene, and R.K. Grzywacz
University of Tennessee

M.A. Bychkov, E. Frlež and D. Počanić (Spokesman)
University of Virginia

29 July 2005

Abstract: We propose to perform a precise measurement of a, the electron-neutrino correlation parameter, and b, the Fierz interference term in neutron beta decay, at the Fundamental Neutron Physics Beamline at the SNS, using a novel electric/magnetic field spectrometer and detector design. The experiment is aiming at the 10^{-3} accuracy level in a, and will provide an independent measurement of $\lambda = G_A/G_V$, the ratio of axial-vector to vector coupling constants of the nucleon. We will also perform the first ever measurement of b in neutron decay, which will provide an independent limit on the tensor weak coupling.

1. Scientific motivation

Neutron β decay, $n \to pe\nu_e$, is one of the basic processes in nuclear physics. Its experimental study provides the most sensitive means to evaluate the ratio of axial-vector to vector coupling constants $\lambda = G_A/G_V$. The precise value of λ is important in many applications of the theory of weak interactions, especially in astrophysics; e.g., a star's neutrino production is proportional to λ^2. More precise measurements of neutron β-decay parameters are also important in the search for new physics. Measurement of the neutron decay rate Γ, or lifetime $\tau_n = 1/\Gamma$, allows a determination of V_{ud}, the Cabibbo-Kobayashi-Maskawa (CKM) matrix element, independent of nuclear models, because Γ is proportional to $|V_{ud}|^2$, as seen in the leading order expression:

$$\Gamma = \frac{1}{\tau_n} = \frac{f^R m_e^5 c^4}{2\pi^3 \hbar^7} \left(|G_V|^2 + 3|G_A|^2\right) \propto |G_V|^2 \left(1 + 3|\lambda|^2\right) = |V_{ud}|^2 \, |g_V|^2 \, G_F^2 (1 + 3|\lambda|^2)\,, \quad (1)$$

where $f^R = 1.71482(15)$ is a phase space factor, m_e is the electron mass, $g_{V,A}$ the vector and axial-vector weak nucleon form factors at zero momentum transfer, respectively, and G_F is the fundamental Fermi weak coupling constant. While the conserved vector current (CVC) hypothesis fixes g_V at unity, two unknowns, V_{ud} and λ, remain as variables in the above expression for Γ. Hence, an independent measurement of λ is necessary in order to determine V_{ud} from the neutron lifetime. Several neutron decay parameters can be used to measure λ; they are discussed below. Precise knowledge of V_{ud} helps greatly in establishing the extent to which the three-generation CKM matrix is unitary. CKM unitarity, in turn, provides an independent crosscheck of the presence of certain processes and particles not included in the Standard Model (SM) of elementary particles and interactions, i.e., an independent constraint on new physics.

Currently, the most accurate value of the CKM matrix element V_{ud} is obtained from measurements of $0^+ \to 0^+$ nuclear β-decays, the so-called superallowed Fermi transitions [1]. However, the procedure of the extraction of V_{ud} involves calculations of radiative corrections for the Fermi transition in nuclei. Despite the fact that these calculations have been done with high precision (see [2] and references therein), it is impossible to verify the values of these nuclear corrections from independent experiments.

A problem with CKM matrix unitarity at the $2-3\sigma$ level persisted for over two decades in the first row sum; e.g., the 2002 Review of Particle Properties [3] reported values of CKM matrix elements that yield

$$\Delta \equiv 1 - |V_{ud}|^2 - |V_{us}|^2 - |V_{ub}|^2 = 0.0032 \pm 0.0014\,. \quad (2)$$

The situation changed drastically in 2003 and 2004 when a series of experiments at Brookhaven, Fermilab and CERN reported revised values of K_{l3} decay branching ratios which led to an upward adjustment, by about 2.5σ, of the CKM matrix element V_{us} [4, 5, 6]. Without getting into the details of this revolutionary development, it will suffice to note that a revised CKM unitarity check yields [7]

$$\Delta = (3 \pm 14) \times 10^{-4}\,, \quad (3)$$

which indicates that, at least for the time being, the question of the CKM matrix unitarity appears to be closed. However, several questions related to V_{ud} still remain open. Firstly,

it is desirable to have an independent check of the superallowed Fermi nuclear beta decay result. Secondly, a disturbing inconsistency persists between the best results on neutron decay and those on nuclear Fermi decays, as well as within the body of the neutron decay data. Finally, by its nature, neutron decay offers redundant consistency checks whose failure can be an indication of new physics. In order to discuss the last two points we turn to the details of neutron decay dynamics.

Neglecting nucleon recoil, as well as radiative and loop corrections, the triple differential neutron decay rate is determined by the decay parameters a, b, A, B, and D, as shown:

$$\frac{dw}{dE_e d\Omega_e d\Omega_\nu} \propto p_e E_e (E_0 - E_e)^2 \times \left[1 + a\frac{\vec{p}_e \cdot \vec{p}_\nu}{E_e E_\nu} + b\frac{m_e}{E_e} + \langle \vec{\sigma}_n \rangle \cdot \left(A\frac{\vec{p}_e}{E_e} + B\frac{\vec{p}_\nu}{E_\nu} + D\frac{\vec{p}_e \times \vec{p}_\nu}{E_e E_\nu} \right) \right], \quad (4)$$

where $p_{e(\nu)}$ and $E_{e(\nu)}$ are the electron (neutrino) momenta and energies, respectively, E_0 is the electron energy spectrum endpoint, and $\vec{\sigma}_n$ is the neutron spin. The "lowercase" parameters: a, the electron–neutrino correlation parameter, and b, the Fierz interference term, are measurable in decays of unpolarized neutrons, while the "uppercase" parameters, A, B, and D, require polarized neutrons. All except b depend on the ratio $\lambda = g_A/g_V$, in the following way (given here at the tree level):

$$a = \frac{1 - |\lambda|^2}{1 + 3|\lambda|^2}, \qquad A = -2\frac{|\lambda|^2 + Re(\lambda)}{1 + 3|\lambda|^2}, \qquad B = 2\frac{|\lambda|^2 - Re(\lambda)}{1 + 3|\lambda|^2}, \qquad D = \frac{2\, Im(\lambda)}{1 + 3|\lambda|^2}. \quad (5)$$

Here we have allowed for the possibility of a complex λ, i.e., a nonzero value of D, the triple correlation coefficient, which would arise from time reversal symmetry violation in the process. Since measurements of D are consistent with zero [1], we will treat λ as real. Given that $\lambda \simeq -1.27$, parameters A and a are similarly sensitive to λ:

$$\frac{\partial a}{\partial \lambda} = \frac{-8\lambda}{(1 + 3\lambda^2)^2} \simeq 0.30, \qquad \frac{\partial A}{\partial \lambda} = 2\frac{(\lambda - 1)(3\lambda + 1)}{(1 + 3\lambda^2)^2} \simeq 0.37, \quad (6)$$

while B is relatively insensitive:

$$\frac{\partial B}{\partial \lambda} = 2\frac{(\lambda + 1)(3\lambda - 1)}{(1 + 3\lambda^2)^2} \simeq 0.076. \quad (7)$$

Experimental status of the above parameters is summarized in the Particle Data Group's review in ref. [1]. It has been true for some time that by far the best precision in extracting λ has been achieved in measurements of A, the correlation between the electron momentum and neutron spin. However, the experimental status of A and λ is far from satisfactory, as shown in Fig. 1. In both cases the error on the weighted average value was rescaled up by a factor of 2 or more because of an uncommonly bad χ^2 value and low confidence levels for the fits and extracted weighted averages. It is particularly disturbing that the most accurate measurement to date, that made by the PERKEO II collaboration [8], is in significant disagreement with the remaining world data set. This disagreement carries over naturally to the value of V_{ud} [1].

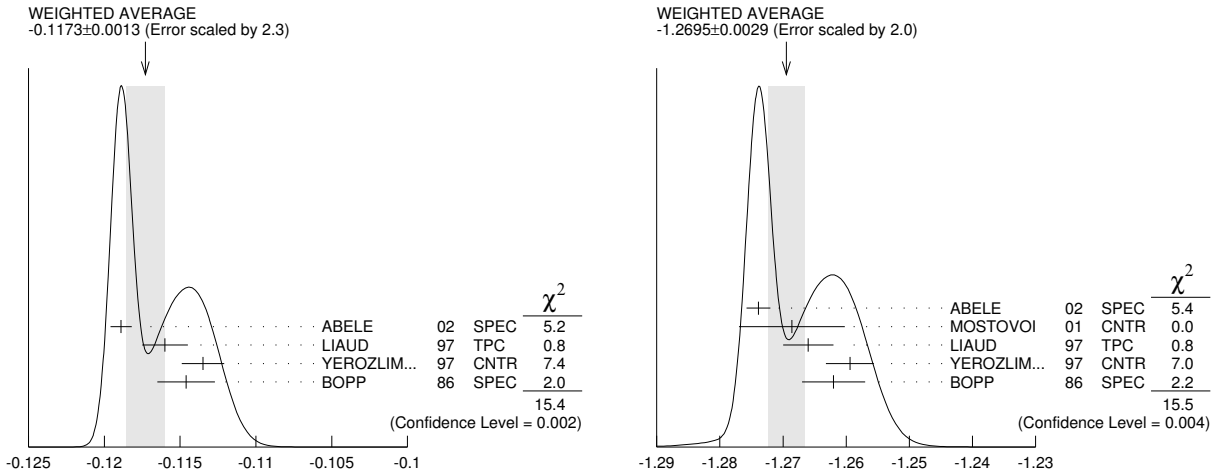

Figure 1: Particle Data Group's 2004 compilation of experimental values of A (left panel) and λ (right panel), see ref. [1]

Present inconsistencies in the value of A must, and will be, resolved by new measurements. Meanwhile, parameter a offers an independent measure of λ with comparable sensitivity and radically different systematics. The latter is entirely devoid of uncertainties associated with neutron polarization, usually the most challenging aspect of a measurement of A. The current world average value of $a = -0.103 \pm 0.004$ is dominated by two 5 % measurements [9, 10], to be compared with the 0.06 % measurement of A in PERKEO II [8].

We are proposing to make a measurement of the e–ν_e correlation parameter a with an accuracy of a few parts in 10^3 using a novel 4π field-expansion spectrometer in the FNPB line at the SNS. The spectrometer and our measurement method are discussed in detail in the next section. The experiment, which we have named 'Nab', will also produce the first measurement of b, the Fierz interference term; to date b has not been measured in neutron decay.

The Nab experiment constitutes a first phase of a program of measurements that will continue with a second-generation experiment named 'abBA', which will measure the polarized neutron decay parameters A and B in addition to a and b. A separate Letter of Intent is being submitted for abBA. Together, the two experiments form a complete program of measurements of the main neutron decay parameters in a single apparatus with shared systematics and consistency checks.

The scope of the Nab experiment extends well beyond resolving the remaining λ and V_{ud} inconsistencies. The relevance of precise determination of beta decay parameters, in particular those of the neutron, to searches for signals of physics beyond the Standard Model has been recently discussed in great detail by Herczeg in ref. [11]. At the proposed accuracy level, parameter a can be used to constrain certain left-right symmetric models (L-R models) as well as leptoquark extensions to the SM. The latter would also be constrained by our measurement of b which is sensitive to a tensor weak interaction that has often been linked to leptoquarks. There have also been proposals of models relying on a new anomalous chiral boson to account for a tensor interaction [12]. The sensitivities of a to, e.g., L-R model

parameters $\bar{a}_{RL}$, $\bar{a}_{RR}$, etc., are competitive and complementary to those of A and B. A general connection between non-SM (e.g., scalar, tensor) $d \to ue\bar{\nu}$ interactions on the one hand, and upper limits on the neutrino mass on the other, was recently brought to light [13], providing added motivation for more precise experimental neutron decay parameters.

2. Technical approach

We propose to measure the electron-neutrino correlation in neutron beta decay, a, using a novel approach. Coincidences between electrons and protons are detected in a field-expansion spectrometer. The function of the spectrometer is to measure the magnitude of the proton momentum, p_p. The electron–neutrino correlation, a, expresses the dependence of the decay rate on the angle between the neutrino and electron,

$$\cos\theta_{e\nu} = \cos\theta_e \cos\theta_\nu + \sin\theta_e \sin\theta_\nu \cos(\phi_e - \phi_\nu)\,. \tag{8}$$

It is not necessary to measure all the above angles because $\theta_{e\nu}$ can be determined from the electron energy and the proton momentum squared. The electron energy is measured precisely in the Si detectors. The electron and neutrino momenta, p_e and p_ν, respectively, can be determined from the electron energy. The quantity $\cos\theta_{e\nu}$ can then be determined from the proton momentum and the electron energy using

$$p_p^2 = p_e^2 + 2p_e p_\nu \cos\theta_{e\nu} + p_\nu^2\,. \tag{9}$$

For a perfect determination of the proton momentum, p_p and $\cos\theta_{e\nu}$, the error in a becomes

$$\sigma_a^{\min} = \sqrt{\frac{3}{n\beta_{ave}^2}} = \frac{2.3}{\sqrt{n}}\,. \tag{10}$$

The reference P configuration design, described below, achieves $\sigma_a = 2.7/\sqrt{n}$.

The basic concept of the spectrometer consists of a superconducting solenoid with its longitudinal axis oriented normal to the neutron beam, which passes through the center of the solenoid. The strength of the solenoidal magnetic field at the position of the neutron beam is 4 T, expanding to 1 T at either end of the solenoid. Inside the solenoid is a second concentric cylindrical solenoid plus an electrode maintaining the neutron decay region at a potential of +30 kV with respect to the ends of the solenoid where detectors are placed at ground potential.

The magnetic field strength is sufficiently high that both the electrons and protons from neutron decay are constrained to spiral along the magnetic field lines with the component of the spiral motion transverse to the field limited by cyclotron radii of the order of one to a few millimeters.

Thus, two segmented Si detectors, one at each end of the solenoid, view both electrons and protons in an effective 4π geometry. The time of flight between the electron and proton is accurately measured in a long, $\sim$ 1.5 meter, drift distance. The electron energy is accurately measured in the Si detectors. The proton momentum and electron energy determine the electron–neutrino opening angle. We have shown that by sorting the data on proton time

of flight and electron energy, a can be determined with a statistical accuracy of $\sim 2.7/\sqrt{n}$, where n is the number of decays observed.

In addition to excellent statistical sensitivity, the approach has a number of advantages over previous measurements. The acceptance of the spectrometer is 4π for both particles. Thin-dead-layer segmented Si detectors as well as all other components in the apparatus, are commercially available. There are no material apertures to determine the acceptance of the apparatus. The charged particles interact only with electric and magnetic fields before striking the detectors. Coincident detection of electrons and protons reduces backgrounds, and allows the *in situ* determination of backgrounds. A time of flight spectrum is obtained for each electron energy. Different parts of the spectra have different sensitivities to a. The non-central portions of the time-of-flight spectra that are relatively insensitive to a can be used to verify the accuracy of the electric and magnetic field determinations.

Two configurations of the spectrometer will be used, the "P" and "PZ". The P configuration of the field-expansion spectrometer is designed to make the momentum of the proton inversely proportional to the proton time of flight, $|\vec{p}_{\rm p}| \propto 1/{\rm TOF}$. In the PZ configuration, $|p_{{\rm p},z}| \propto 1/{\rm TOF}$, i.e., the PZ configuration measures only one component of the proton momentum and therefore has a larger statistical uncertainty than the P configuration. On the other hand, in the P configuration there is a small probability ($\sim 0.3\,\%$) that the momentum direction will be reversed and the TOF increased. By using both configurations we will be able to check on errors associated with field mapping and other systematic uncertainties.

A not-to-scale design for the P configuration of the field expansion spectrometer is shown in Fig. 2. Electrons and protons spiral around magnetic field lines and are guided to two 10 cm by 10 cm segmented Si detectors. In the center of the spectrometer the field strength is 4 T, in the drift region 0.2 T, and near the Si detectors 1 T (see Fig. 3). As also shown in Fig. 3, in the PZ configuration, the magnetic field is maintained at 4 T over almost the entire TOF path. The field expansion decreases the angle between the momentum and the magnetic field lines. The velocity in the drift region is close to $|\vec{p}|/m$. The particles strike the detectors at approximately normal angles, thus reducing the probability of backscattering. An electric field is applied to the particles before they strike the Si detectors so that the protons have enough energy to be detected, while the energy of the electrons is reduced. The electric field must be applied after the magnetic field expansion so that the electrons acceptance does not depend on electron energy. For the reference design, all electrons that have energies above 70 keV reach the detectors and deposit at least 30 keV. After the drift region the protons are electrostatically accelerated from $\sim$ 400 eV to 30 keV as they cross a narrow gap in the cylindrical electrode so that the time spent between the potential change and the detector is small compared to the time spent in the drift region. Electrons may be scattered from the Si detectors, but scattered electrons are guided back to one of the detectors and eventually all of the electrons' energy is deposited in the detectors.

Because the charged particle trajectories are constrained to follow the magnetic field lines, the segmented Si detectors form a projected image of the beam. The ends of the decay region are defined by the image of the beam on the detectors. The transverse migration of back scattered electrons is small because the radius of gyration is small, a few mm, and because the momentum of the electron decreases with each reflection.

The event count rate at the SNS at 1.4 MW operation is 19.5 counts/sec/cm^3 of fiducial

volume. A $16\,\mathrm{cm}^3$ fiducial volume is easily attainable leading to an event rate of 310 Hz. For example, the electron-neutrino correlation can be determined with a statistical uncertainty of 0.2 % in a typical run of 7×10^5 s, or about ten days. We plan to have several such runs, ideally in both P and PZ configurations, thus further substantially reducing the uncertainties. The statistical uncertainty in a would be .0006 as compared to .003 in the Particle Data Listings. As discussed in the preceding section, the uncertainty in G_A/G_V in the Particle Data Listings is based on inconsistent data on A, the electron-spin correlation in neutron beta decay.

The hermetic nature of the electron energy measurement provides a clean and precise measurement of the electron energy spectrum, leading to an excellent determination of b, the Fierz interference term. The Fierz interference term, never before measured in neutron decay, modifies the shape of the electron spectrum. The statistical uncertainty in b is higher than that for a, because the quantity m/E_e is strongly correlated with the normalization of the beta spectrum for kinetic energies larger than approximately half the electron mass. The statistical uncertainty in b is given by $\Delta b_\mathrm{stat} = 5.9/\sqrt{n}$ for an electron energy threshold of 0.1 MeV. Hence, in a typical 7×10^5,s run we would expect $\Delta b_\mathrm{stat} \sim 4\times10^{-4}$. The $V-A$ Standard Model predicts $b=0$. We expect to collect several samples of 10^9 events in several 6-week runs. The large event rates make it possible to study systematic uncertainties and achieve small statistical uncertainties in moderate run times.

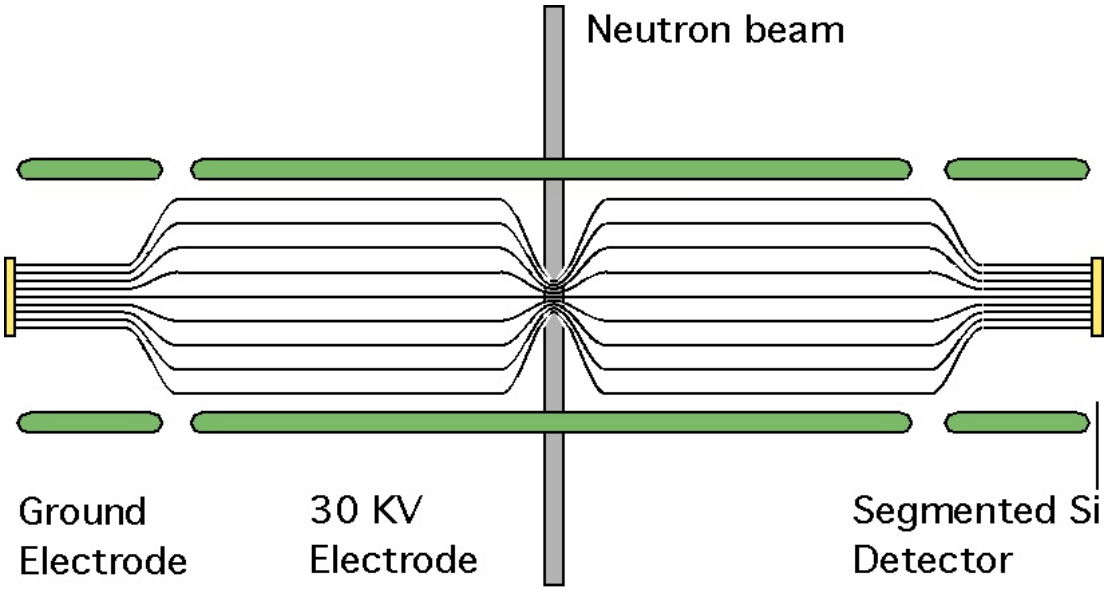

Figure 2: A schematic view of the field expansion spectrometer.

To date, the best information on G_A/G_V has come from measurements of A, the electron–neutron spin correlation. In order to measure A it is necessary not only to determine the neutron polarization, but also which of the two detectors the electron struck first. This determination may be imperfect due to electron back-scattering. The electron–neutrino opening angle depends on the square of the proton momentum and it is therefore not necessary to determine the relative direction of the electron and proton in order to measure the electron–neutrino correlation; the TOF and electron energy are sufficient. The practical implication of

combining the two directions is important. It is possible to obtain commercially segmented Si detectors with thin ion-implanted entrance windows. The large sheet resistance of the ion-implanted junction and the large rise time ($\sim$ 50 ns) make fast timing difficult. The ability to use slow Si detectors makes the experiment feasible without having to resort to new technology.

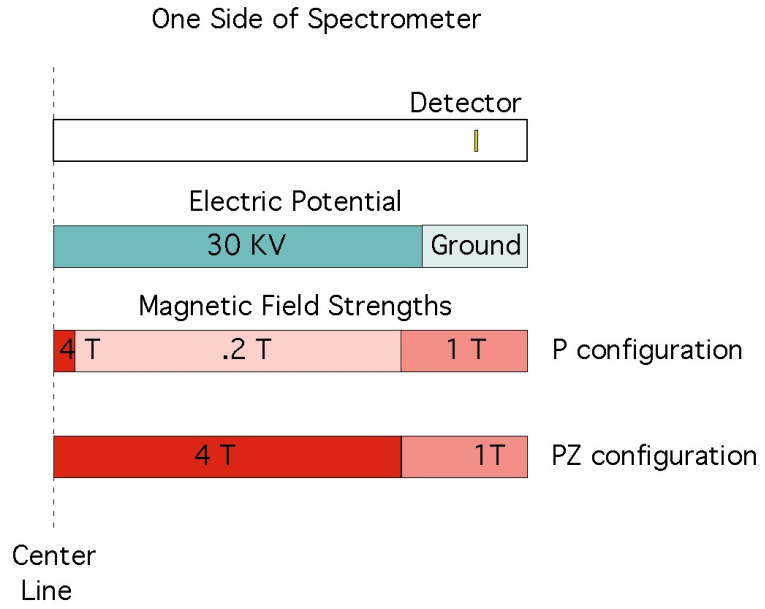

Figure 3: Scale drawing of one side of the field-expansion spectrometer for the P and PZ configurations. In the P configuration, the proton momentum is longitudinalized by the field expansion and $|\vec{p}_{\rm p}| \propto 1/{\rm TOF}$. In the PZ configuration the z component of the proton momentum is unchanged until the field expands just before the electric acceleration, and $|p_{{\rm p},z}| \propto 1/TOF$. The distance from the center of the spectrometer to either detector is 2 m.

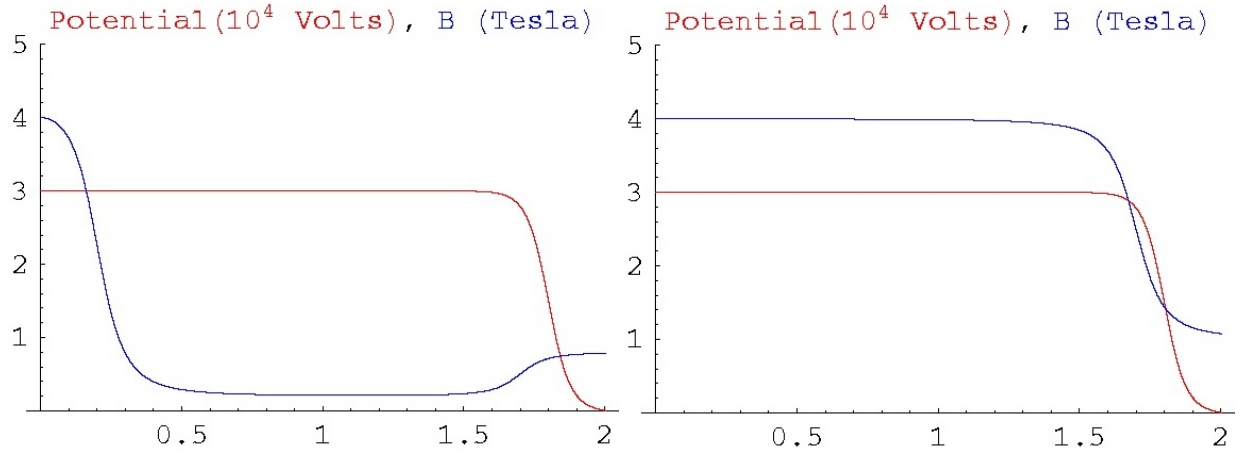

Figure 4: Electric potential and magnetic field on the spectrometer axis for the P configuration (left) and PZ configuration (right).

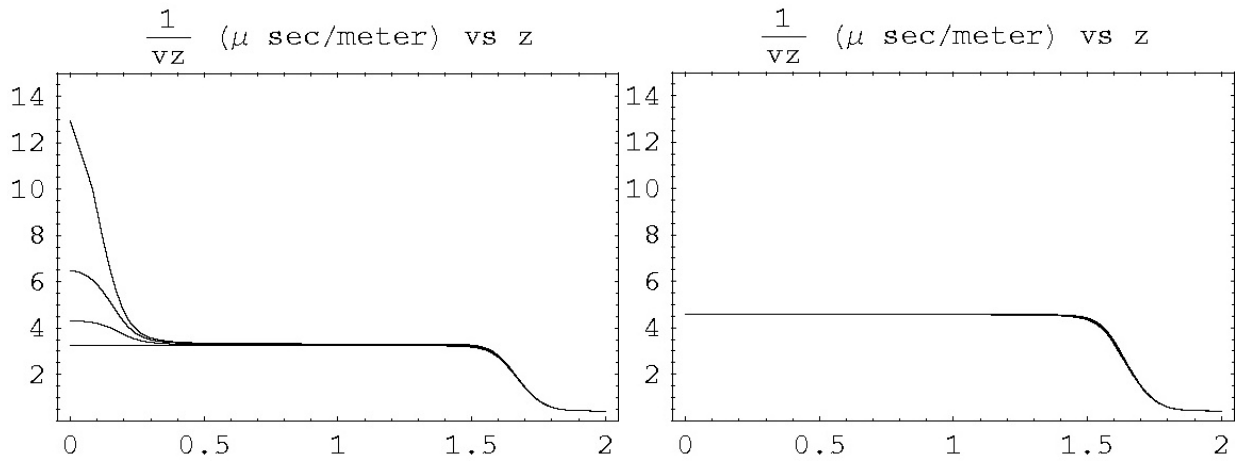

Figure 5: Inverse proton velocity z-component versus position in spectrometer for the P configuration (left) and PZ configuration (right). We note that TOF $= \int dz/v_z$. For the P configuration $p_{\rm p}$ is fixed; the four curves correspond to $p_{{\rm p},z}$ having values of 0.25, 0.50, 0.75, and 1.00 times $|\vec{p}_{\rm p}| = p_{\rm p}$. Proton time of flight depends primarily on on $p_{\rm p}$. For the PZ configuration, four values of $p_{\rm p}$ span the kinematically allowed range, while $p_{{\rm p},z}$ is fixed. The four curves are nearly indistinguishable, and there is a close relationship between $p_{{\rm p},z}$ and time of flight. For both configurations, at $z \sim 1.65\,{\rm m}$ the electric field accelerates the proton to 30 kV and $1/v_z$ becomes small.

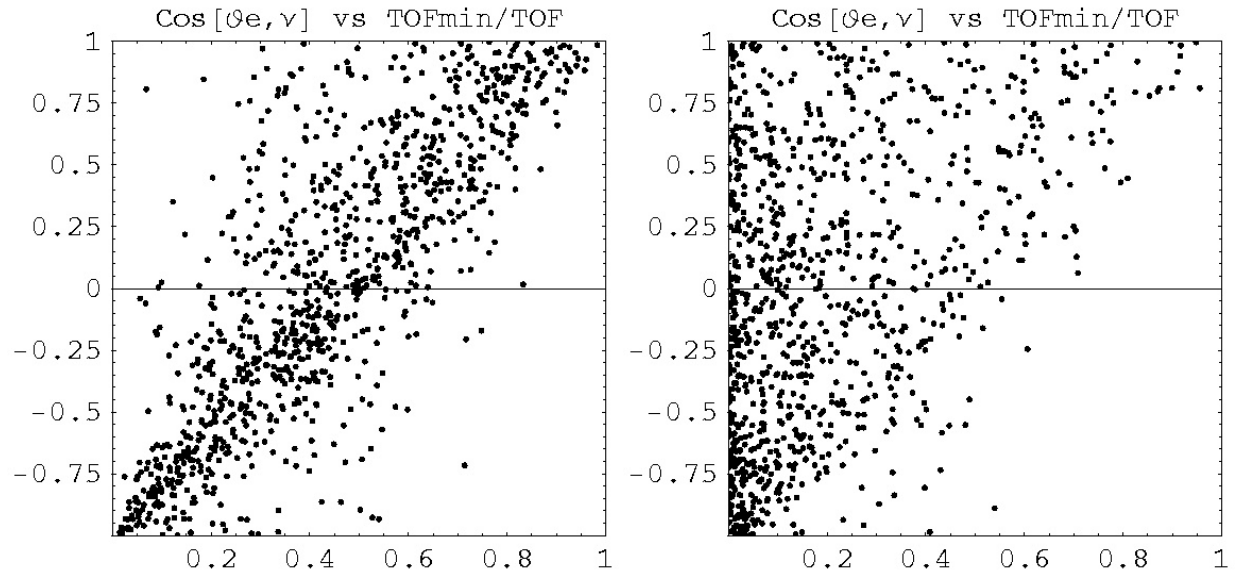

Figure 6: Scatter plots of $\cos\theta_{{\rm e}\nu}$ versus the ratio ${\rm TOF}_{\rm min}/{\rm TOF}$ for the P configuration (left) and the PZ configuration (right). The correlation between TOF and the electron–neutrino opening angle is large for the P configuration and smaller for the PZ configuration.

In order to optimize our design and study the systematics in detail, we have developed a realistic Monte Carlo simulation of the spectrometer using the standard CERN package GEANT4 [14]. This approach allows us to evaluate with high precision the effect of changes or uncertainties of any parameter in the apparatus. While our Monte Carlo work and spectrometer optimization are in their early stages, we illustrate some of the salient features of the apparatus below. Fig. 7 shows typical magnetic field profiles for the P and PZ configuration, respectively. Fig. 8 shows two possible configurations of the electric field, corresponding to the accelerating potential before (1) and after (2) the magnetic field expansion. The effect of these field configuration choices on the signal for the parameter a is illustrated in Fig. 9

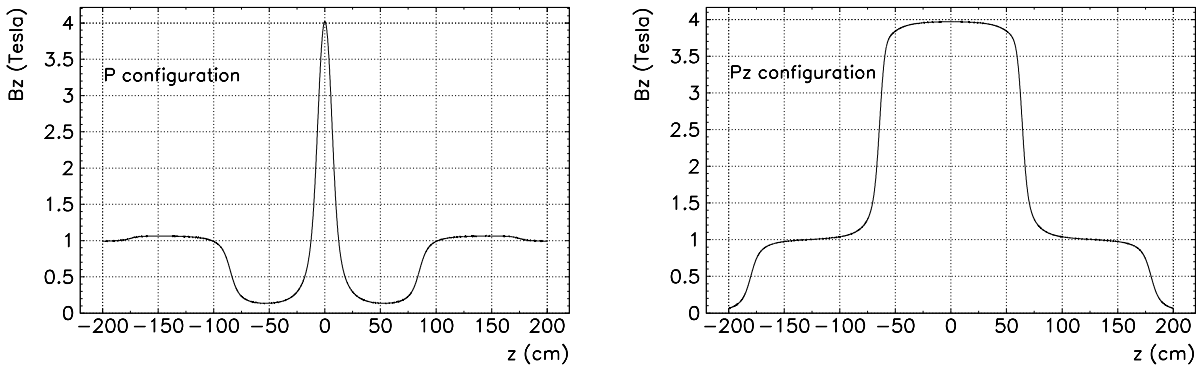

Figure 7: Magnetic field z-coordinate profiles for prototype P (left) and PZ (right) compact spectrometer configurations currently used in the GEANT4 Monte Carlo simulations. The Si detectors are placed at $z = \pm 125\,\mathrm{cm}$.

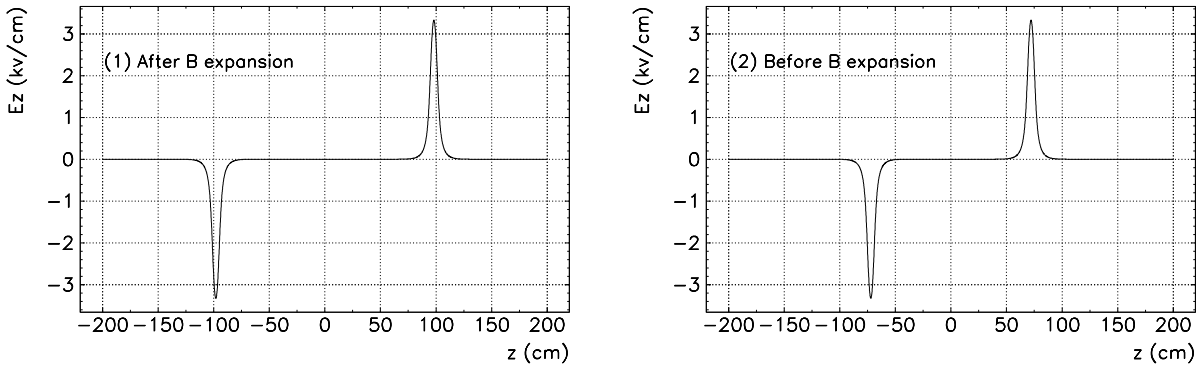

Figure 8: Two electric field z-coordinate profiles currently used in the GEANT4 Monte Carlo simulations: (1) placing the accelerating potential after (left panel), and (2) before (right panel) the magnetic field expansion depicted in the preceding figure.

which shows the distortion of the proton TOF spectrum due to a one percent increase in the decay parameter a that would be recorded in one typical run ($7 \times 10^5\,\mathrm{s}$, or $\sim 2 \times 10^8$ neutron decay events) in two P and PZ configurations. Fig. 9 illustrates several points.

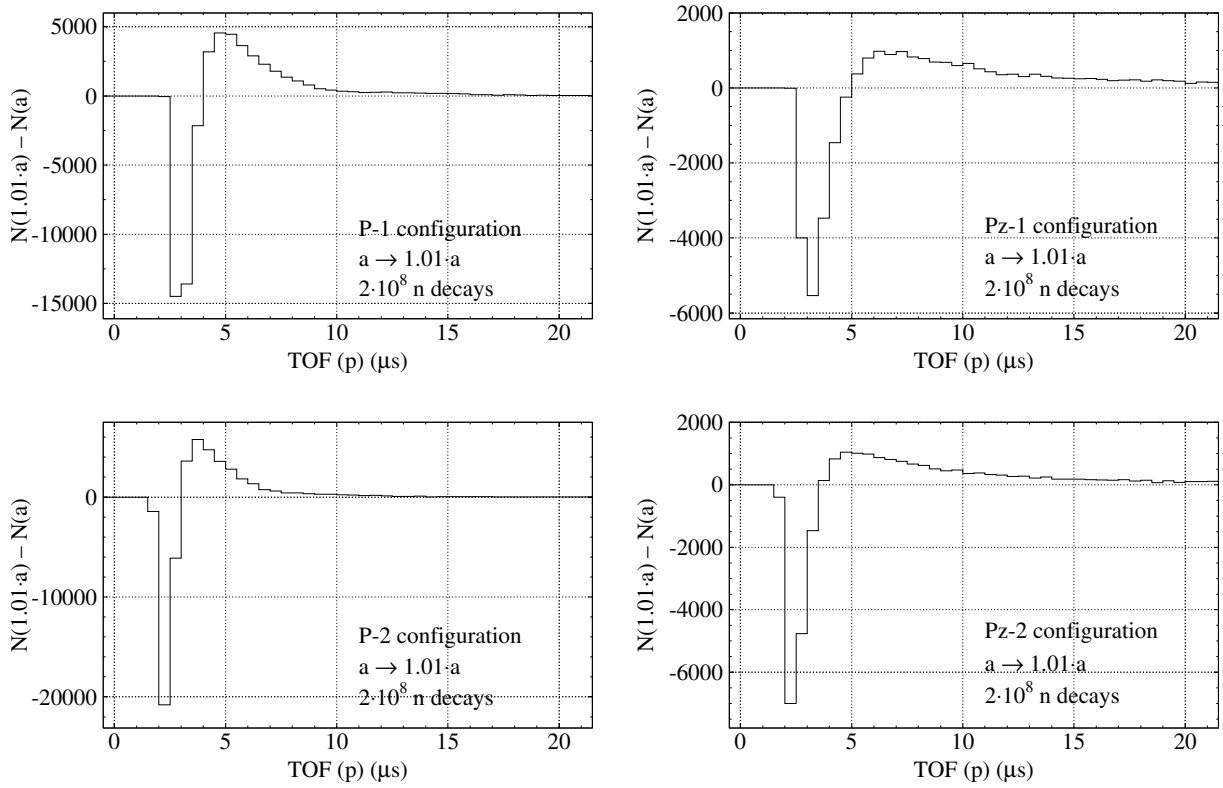

Figure 9: Distortion of the observed proton TOF spectrum, $N_{\rm obs} - N_{\rm nominal}$, as a function of proton time of flight TOF(p) in μs, for the electron-neutrino correlation parameter value $a = 1.01 \cdot a_{\rm nominal}$, in a typical run with $N \sim 2 \times 10^8$ neutron decay events. The B, E field configurations are listed as P-1, PZ-1, etc.

First, increasing the size of the electron-neutrino correlation parameter a has the effect of softening the proton spectrum. Second, the P field configurations provide greater sensitivity to a than the PZ configurations. However, we are considering using both because doing so offers important checks of systematic errors. Third, each histogram shown in Fig. 9 results from a subtraction of two large and nearly equal spectra, $N_{\rm obs}$ and $N_{\rm nominal}$, each containing a total of 2×10^8 events. The associated statistical uncertainties are large—for the most important, early TOF bins the uncertainty is of the order of several thousand counts per bin. Thus, a run with 2×10^8 neutron decays is statistically sensitive at the level of about 1 %, or so, in a. This illustrates just how hard the measurement of a is, and provides the reason why we need to collect a sample of several billion events in order to reach the desired sensitivity. Finally, the proton TOF histograms shown here were not constrained by any cuts on electron energy. Imposing appropriate cuts on $E_{\rm e}$ can enhance the relative sensitivity to a by up to 30 %, which is significant.

The last point illustrates an important feature of the proposed experiment. While a measurement of a mainly requires the proton TOF information and uses the electron signal primarily as a time marker, measurement of b relies entirely on a precise determination of the electron energy spectrum. In this way, the two measurements are complementary. Accurate

measurements of both proton TOF and electron energy provide us with means to evaluate multiple independent cross-checks of the systematic uncertainties in both a and b.

3. The detector

The detector design is a challenging issue for the neutron beta-decay experiment. The detector has to be able to stop and detect the full full energy of 50–750 keV electrons as well as 30 keV protons. This requires the detector thickness to be about 2 mm Si-equivalent, a very thin window technology, and very low energy threshold for detecting signals down to about 15 keV.

The very thin window/dead-layer should uniformly cover a large area of $\approx 100\,\mathrm{cm}^2$. The detector has to be segmented into about 100 elements. The segmentation has to be applied on the back side to keep the irradiated front side homogeneous. The segmentation is necessary to determine the particle position and thus identify the electron/proton trajectory. The time and spatial pattern of electron energy deposition has to be measured. The detector segmentation has to be combined with pulse processing electronics allowing for the real time signal recording with a resolution at the level of few ns. The low energy threshold is related to a good energy resolution, at the level of few keV for the relevant energy range of electrons and protons.

The liquid nitrogen cooled silicon detector has the ultimate efficiency stability and energy resolution unsurpassed by any other type of detector.

The design goal, pursued in a collaboration with Micron Semiconductor Ltd., is to build a large area segmented single wafer silicon detector, about 2 mm thick to enable stopping the electrons, and operating with a liquid nitrogen cooling at the temperature level of about 100 K. The readout will be implemented using cold-FET preamplifier and real-time digital signal processing electronics.

The detector which fulfill all the experimental requirements was not manufactured yet, but the technology required to build such detector is well developed. The collaboration has taken several steps in order to test the specific features based on commercially available detectors.

3.1. Si(Li) detectors

Two liquid-nitrogen cooled small area Si(Li) spectrometers were used to perform initial tests with mono-energetic electrons source of ^{207}Bi. These $200\,\mathrm{mm}^2$ area, 5 mm thick Si(Li) crystals have 20nm Si-equivalent thin window, corresponding to about 3 keV energy loss for 30 keV protons. The energy resolution measured as a Full Width of Half Maximum (FWHM) for 970 keV electrons is about 1.8 keV. The 5 mm thickness allows to stop up to 2 MeV electrons. Such standard detectors fulfill all requirements of neutron beta decay experiment except for the size and segmentation.

Therefore, a construction of new spectrometer based on a $900\,\mathrm{mm}^2$ segmented Si(Li) crystal is pursued. This nine-segment 3 cm by 3 cm rectangular Si(Li) crystal has been delivered by Eurisys-Canberra Industries, see Fig 10. The 5 mm thick detector has the segments on the back and uniform 200-nm front layer. The back-side only segmentation effectively results in elimination of dead-zones between the segments.

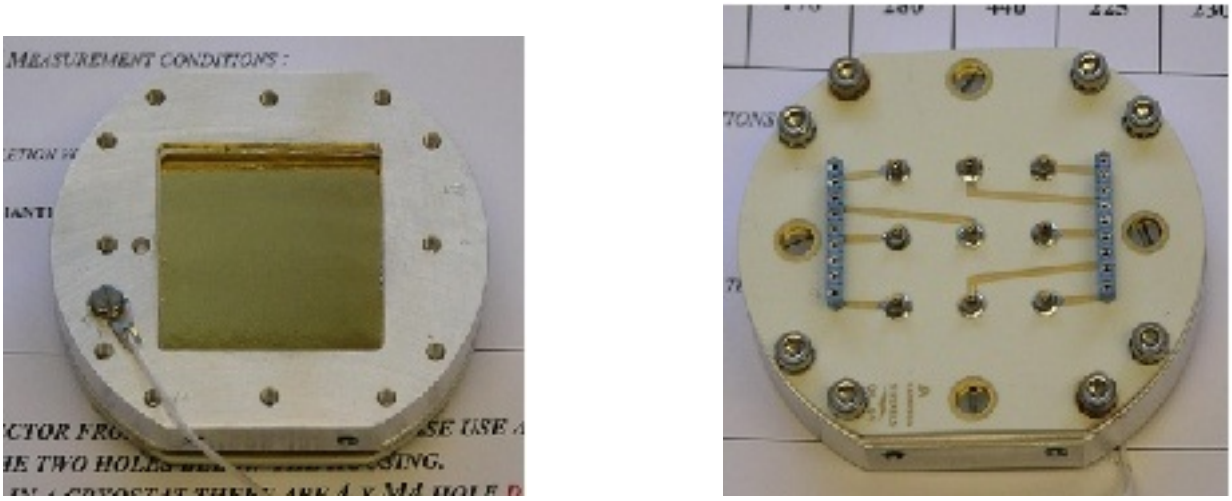

Figure 10: The view of the front side (left) and back side (right) of the 9 cm^2 segmented Si(Li) detector. All nine contacts, one per segment, can be seen on the back.

The detector will be outfitted with nine standard Canberra preamplifiers and all nine FETs will be nitrogen cooled. The resolution of about 2 keV (FWHM) at 1 MeV is expected. This detector is a platform to test the technical issues related to the segmentation like compact FET mount and cooling. It also will be used to develop the triggering schemes, mainly to test the add-back between the segments.

3.2. Segmented Si detectors

The application of Double-sided Silicon Strip Detectors coupled to the digital electronics to the charge-particle spectroscopy is an area of expertise of the ORNL team, see, e.g., Refs. [15, 16]. The Micron DSSDs, of BB1 design [17], having 40 by 40 strips, 1 mm wide, are commonly used in the experiments at the Holifield Radioactive Ion Beam Facility (HRIBF). These detectors, with the thicknesses from 65 microns up to 1.5 mm, and sizes up to 50 mm by 50 mm, are already available and tested at the HRIBF. These detectors are typically cooled down to about -35°C and have energy resolution of about 18 keV FWHM for 1 MeV protons.

Recently the technique of ultra-thin 100 nm windows has been developed for a Micron DSSD detector [18]. Such a thin layer covers over 97% of the detector, while a good conductivity of the electrodes is provided by the Al mesh made out of 30 μm wide strips, spaced every 1.5 mm of the detector surface. Two detectors made with such thin window technology were acquired from Micron. These are 1.5 mm thick, 50 by 50 mm counters of W1-design have 16x16, 3 mm wide strips, see Fig. 11. These W1 detectors are currently being tested at the HRIBF.

Larger detectors with radial and azimuthal segmentations are in common use in experimental studies. However they may not be available in the 100-pad configuration. This is not a technological impediment. The final detector has to combine the existing technologies of manufacturing large, thick segmented Si (or Si(Li)) detectors with ultra-thin window with the possible use of the mesh-type contact. The uniform liquid nitrogen cooling and

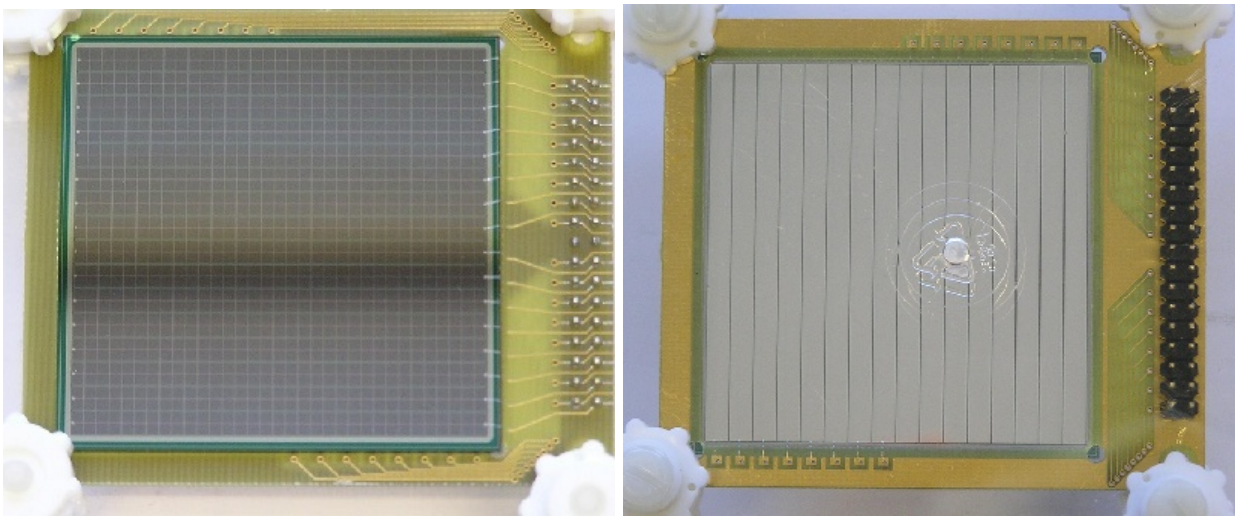

Figure 11: View of the front side (left) and back side (right) of the 16 by 16 strips DSSD detector. Thin aluminum mesh improving the conductivity is visible on the front.

its compactly mounted FET with nine 1 cm^2 segment Si(Li) crystal will be available for commissioning within next few months. The next generation - large area, 100-pad detector remains to be developed and tested.

4. Potential systematic uncertainties in the measurement of a, b

1. Magnetic field map

   If we use incorrect magnetic or electric field values, we will calculate the nominal TOF incorrectly, distorting the signal for a (see Fig. 9). Fig. 12 shows the sensitivity of the quantity $1/v_z$ (we recall that proton TOF $= \int dz/v_z$) on the magnetic field strength in the P and PZ configurations.

2. Hermiticity ($E_{\rm e}$)

   If some electron energy is lost, we will reconstruct the electron energy spectrum and the $\theta_{e\nu}$ incorrectly. Electron energy can be lost (a) due to the non-zero radii of gyration of the electron orbits, and (b) in dead detector layers.

   a. Electron walk caused by scattering in detector and non-zero radii of gyration: If the magnetic field were normal to the Si detector surface and the electron reflected elastically from the detector, the electron would follow its original guiding center. However, the electron loses energy and all three components of momentum change. The electron may then fall outside of the guarded area of the detector. We have estimated the walk and found it to be small compared to the size of a detector, $\sim 1\,$cm.

   b. The electron energy loss in the detector dead layer will be very small. We require proton energy loss of $< 5\,$keV. The electrons' energy losses are $\sim$ 2000 times smaller than the protons'.

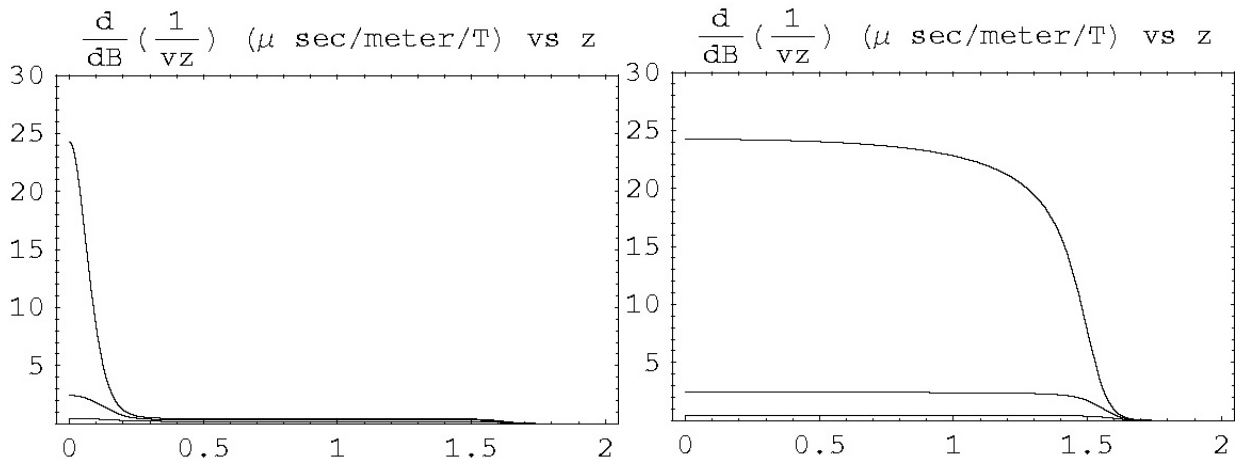

Figure 12: Sensitivity of the quantity $1/v_z$ to the magnetic field strength for $p_z = .25$, .5, .75, and $1.0\,p$. The error in the calculated TOF is the quadratic sum of the field measurement errors weighted with the sensitivity. The sensitivity for the P configuration (left) is large where the field is large, and decreases for large values of z where the proton momentum has been longitudinalized. The sensitivity in the PZ configuration (right) is large up until the field expansion and application of the electric field.

3. Electron energy calibration

   If the individual pixels are not all correctly calibrated, errors in the electron energy will result. We will calibrate the pixels using the end point of the neutron beta decay spectrum. If the spectrometer is filled with a low pressure of ^{3}He, the neutron beam will interact producing a flux of back-to-back monochromatic p–^{3}H events that have the same source distribution as the neutron beta decay events. These p–^{3}H events provide 2 lines, at 198 and 594 keV, which can be used to calibrate the energy response and align the detector.

4. Trigger hermiticity

   If we lose events, the data set will be biased. We will determine a value of a from a subset of the total number of neutron beta decay events, since a does not depend uniformly on the decay phase space. The best approach is to trigger on every proton event in order to avoid a bias in the data sample. The protons are expected to have between 30 and 30.8 keV from the 30 keV accelerating potential and the initial proton kinetic energy. The loss in the dead layer is ~ 5 keV. The back-scattering probability for protons from Si is very small. Furthermore, protons that lose more than 800 eV in the dead layer are forced back into the same detector by the electric field. Every proton deposits ~ 25 keV in one or the other detector. We can therefore trigger on every event that deposits more than a lower threshold of, say, 10 keV, and less than an upper threshold of, say, 50 keV.

5. TOF uncertainties

   We will measure the difference between the proton and electron TOF's. The electron

TOF is a few times 10 ns, and the proton TOF is several μs. The statistical uncertainty is dominated by the 25 keV proton signal, and we expect TOF resolution of under 5 ns, more than sufficient for the task at hand. Corrections due to time dispersion are small, $\sim (\sigma^{\rm TOF}/TOF)^2 < 10^{-5}$. Several effects modify the TOF; among them we note:

a. reflection of the electron or proton in the field pinch near the beam,

b. sub-threshold electron reflections.

a. If an electron (or proton) is created with a small p_z and is headed into an increasing magnetic field strength, it may be reflected. We estimate the reflection probability to be a few $\times 10^{-3}$. The path length changes due to reflections are a small fraction of the total path length, but must be modeled.

b. Problems arise if an electron is reflected but deposits insufficient energy to be detected. The TOF error is given by the additional time it takes the electron to strike either detector. Longitudinalizing the electron momentum minimizes this problem. We will model the probability of reflection and apply a correction. We can evaluate this problem *in situ* by analyzing the data with different electron thresholds and extrapolating to zero threshold. The form of the extrapolation must match a calculation based on the field map and multiple scattering Monte Carlo code (GEANT, EGS).

6. Timing spread due to non-zero beam size

   The beam size will be ~ 2 cm in the decay region. A beam size of 2 cm produces a small effect on the TOF spectrum. This change can be accurately modeled from the field map and source distribution. The source size can be measured from the p–^{3}H data.

7. Proton hermiticity and uniformity

   Detecting every proton eliminates trigger bias and helps control the systematics. This is facilitated by our spectrometer which makes all protons monoenergetic, each depositing 30 keV in the detector. The detector should therefore have a uniform front surface – no grids or other inhomogeneities. An aluminum conduction deposit is better than a gold conducting deposit because there is less back-scattering. The NIST lifetime experiment measured $\sim 1\,\%$ back scattering from Au surface barrier detectors. An aluminum deposit will have a smaller back-scatter probability than an Au deposit.

8. Proton TOF cutoff

   The proton TOF spectrum has a minimum TOF of about 2 μs for a typical design drift distance. For large times, the TOF spectrum falls off as $1/T^2$. The fraction of events lost after a cutoff time, $T_{\rm cut}$ is $\sim T_{\rm min}/T_{\rm cut}$. However, in spite of their intrinsic sensitivity to a, large-TOF events play a limited role in the determination of a because of their relatively low statistical significance, especially in the P configuration, as demonstrated in Fig. 9. This circumstance greatly reduces the impact of the correction due to missed large-TOF events. On the other hand, large-TOF events are valuable for checking details of the spectrometer systematics. We will therefore make the cutoff time as large as practical.

We have initiated a detailed realistic GEANT4 Monte Carlo study of the influence that each of the above effects has on the overall uncertainty. Acquiring quantitative results at the necessary level of precision takes long because a meaningful simulation run must include upwards of a billion events. Strategies for speeding up this process are currently under development. Results of the Monte Carlo analysis will strongly influence our spectrometer design.

5. Summary

We have developed a method for a simultaneous measurement of the neutron decay parameters a, the neutrino-electron correlation, and b, the Fierz interference term, with precision of a few parts in 10^3. The measurement of a would be competitive with the best measurements of the neutron decay asymmetry parameter A. Our proposed measurement of b would be the first ever in neutron decay.

We propose to make the measurements in the Fundamental Neutron Physics Beam Line at the SNS. The experiment will require a dedicated 4π spectrometer with combined electric and magnetic fields, and novel Si detectors. Details of the design of the spectrometer are currently still under development, while work on the Si detectors is well under way. We expect, however, to have final designs in place well before the FNPBL becomes operational, thus enabling Nab to be among the early experiments to use the beamline.

At the time of this writing we are not in a position to give a firm cost estimate for the project due to remaining design uncertainties. We expect, however, to have a preliminary cost breakdown before the end of 2005.

References

1. S. Eidelman et al., Phys. Lett. B **592**, 1 (2004).
2. I. Towner and J. Hardy, Phys. Rev. C **66**, 035501 (2002).
3. F.J. Gilman, K. Kleinknecht and B. Renk, in *"Review of Particle Physics"*, K. Hagiwara et al., Phys. Rev. D **66**, 01001-113 (2002).
4. A. Sher et al. (BNL 865 Collaboration), Phys. Rev. Lett. **91**, 261802 (2003).
5. T. Alexopoulos et al. (KTeV Collaboration), Phys. Rev. Lett. **93**, 181802 (2004).
6. A. Lai et al. (CERN NA48 Collaboration), Phys. Lett. B **602**, 41 (2004).
7. A. Czarnecki, W.J. Marciano, and A. Sirlin, Phys. Rev. D **70**, 093006 (2004).
8. H. Abele et al., Phys. Rev. Lett. **88**, 211801 (2002).
9. C. Stratowa et al., Phys. Rev. D **18**, 3970 (1978).
10. J. Byrne et al., J. Phys. G **28**, 1325 (2002).
11. P. Herczeg, Prog. Part. Nucl. Phys. **46**, 413 (2001).
12. M.V. Chizhov, e-prints hep-ph/0402105, hep-ph/0411098, and references therein.
13. T.M. Ito and G. Prézaeu, Phys. Rev. Lett. **94**, 161802 (2005).
14. http://geant4.web.cern.ch/geant4/

15. R. Grzywacz et al., Nucl. Inst. and Meth. in Phys. Res. **B204**, 649 (2003).
16. M. Karny et al., Phys. Rev. Lett. **90**, 012502 (2003).
17. www.micronsemiconductor.co.uk/products-strip.asp
18. O. Tengblad et al., Nucl. Inst. and Meth. in Phys. Res. **A525**, 458 (2004).